Deliverable Report

Deliverable D1.7

Deliverable Title: OAM methods for nano-probing

(Replacement for original deliverable on "Final cavity-enhanced SPDC")

Grant Agreement number: **255914**

Project acronym: **PHORBITECH**

Project title: **A Toolbox for Photon Orbital Angular Momentum Technology**

Project website address: **www.phorbitech.eu**

Name, title and organization of the scientific representative of deliverable's lead beneficiary (task leader):
Dr Juan P. Torres
ICFO - Institut De Ciencies Fotoniques
Castelldefels, Spain

Deliverable table

Deliverable no.	D1.7
Deliverable name	Final cavity-enhanced SPDC
WP no.	1
Lead beneficiary no.	3 (ICFO)
Nature	P, R
Dissemination level	PU
Delivery date from Annex I	Originally planned: M24; postponed to M36
Actual delivery date	12 October 2013

In the report accompanyying the deliverable D1.7 of September 2012, further research on the use of cavities for the efficient generation of light with OAM was considered of insufficient importance and relevance so as to continue being considered a topic of interest (Deliverable D1.7). As an alternative, it was proposed to demonstrate experimentally two methods aimed at detecting the thickness of nanofeatures, and the movement of small targets, making use of light with orbital angular momentum.

Both works are well inside the Phorbitech spirit (to develop a toolbox and explore new applications of light with OAM), and surely its impact for OAM technologies can be much more important. Both ideas were not envisaged four years ago when the Phorbitech Project was written down. During this third year, we have carried out both experiments.

1) *N. Hermosa, C. Rosales-Guzman, S. Pereira, and J.P. Torres, Experimental demonstration of nanometric layer thickness detection via spatial mode projection, submitted for its publication on 1st October 2013 to the journal Applied Physics Letters (also published on arXiv:1306.0776)*
   We have demonstrated an optical scheme for detecting few nanometers layer thickness detection. In projecting the reflected beam from the sample under investigation onto an array of appropriately tailored spatial modes (*spatial mode projection*), we increase the sensitivty of the method when compared with other methods which detects the amount of energy present in a specific reflected mode. We have demonstrated the detection of layer thickness of up to 9 nm. The method holds promise to detect even subnanometric layer thichkness.

2) *Carmelo Rosales-Guzman, Nathaniel Hermosa, Aniceto Belmonte, and Juan P. Torres, Experimental detection of particle transverse movement with structured light, Scientific Reports, vol. 3 2815 | DOI: 10.1038/srep02815*
   The original idea of this method is described in another Phorbitech paper (Belmonte and Torres, Opt. Lett. **36,** 4437, 2011]. Experimental results have been presented in ICOAM 2013 (see Poster 21: C. Rosales-Guzman, Transverse Doppler effect using optical beams with a twist). This technique can enhance the capabilities of Doppler laser radar systems.

   We firmly believe that these two experiments are of great importance and represent a significant contribution of Phorbitech in this area of research. These are two new applications of the use of light with orbital angular momentum (OAM toolbox) might impact on two fields of great current interest:

   1) Detection of picometer-size surface features

   2) Coherent Laser Doppler systems for the detection of velocities and positions in myriad of fields

PHORBITECH contribution to this deliverable

PHORBITECH in this work has supported the cost of the 12 person-Months positions of Nathaniel Hermosa, 6 Persons-Months positions of Carmelo Rosales-Guzman, a fraction of the salaries of the senior scientists and the purchase of some lab materials.

PHORBITECH contributors to this deliverable

ICFO: Nathaniel Hermosa, Carmelo Rosales-Guzmán, Juan P. Torres

Publications included in this deliverable

1. Carmelo Rosales-Guzman, Nathaniel Hermosa, Aniceto Belmonte, and Juan P. Torres, "Experimental detection of particle transverse movement with structured light", *Scientific Reports*, vol. **3**, 2815 (2013). DOI: 10.1038/srep02815
2. N. Hermosa, C. Rosales-Guzmán, S. F. Pereira, J.P. Torres, "Nanolayer thickness detection via spatial mode projection", arXiv:1306.0776, submitted to Appl. Phys. Lett.

SCIENTIFIC REPORTS

OPEN

SUBJECT AREAS:
IMAGING AND SENSING
APPLIED OPTICS

Received
9 July 2013

Accepted
12 September 2013

Published
2 October 2013

Correspondence and requests for materials should be addressed to J.P.T. (juanp.torres@icfo.es)

Experimental detection of transverse particle movement with structured light

Carmelo Rosales-Guzmán[1], Nathaniel Hermosa[1], Aniceto Belmonte[2] & Juan P. Torres[1,2]

[1]ICFO-Institut de Ciencies Fotoniques, Mediterranean Technology Park, 08860 Castelldefels (Barcelona), Spain, [2]Universitat Politècnica de Catalunya, BarcelonaTech, Department of Signal Theory & Communications, 08034 Barcelona, Spain.

One procedure widely used to detect the velocity of a moving object is by using the Doppler effect. This is the perceived change in frequency of a wave caused by the relative motion between the emitter and the detector, or between the detector and a reflecting target. The relative movement, in turn, generates a time-varying phase which translates into the detected frequency shift. The classical longitudinal Doppler effect is sensitive only to the velocity of the target along the line-of-sight between the emitter and the detector (*longitudinal velocity*), since any *transverse velocity* generates no frequency shift. This makes the transverse velocity undetectable in the classical scheme. Although there exists a relativistic transverse Doppler effect, it gives values that are too small for the typical velocities involved in most laser remote sensing applications. Here we experimentally demonstrate a novel way to detect transverse velocities. The key concept is the use of structured light beams. These beams are unique in the sense that their phases can be engineered such that each point in its transverse plane has an associated phase value. When a particle moves across the beam, the reflected light will carry information about the particle's movement through the variation of the phase of the light that reaches the detector, producing a frequency shift associated with the movement of the particle in the transverse plane.

The classical Doppler effect, i.e., the *longitudinal Doppler effect*, is a key ingredient in myriad of laser remote sensing systems, which are widely used to monitor the location and velocity of moving targets[1]. In a monostatic standard laser remote system, where the transmitter and the receiver are at the same location, the electromagnetic signal that is incident on the moving target is usually characterized as a Gaussian beam which does not show any appreciable phase dependence in the transverse spatial coordinates. The beam reflected by the target will have a time-varying phase given by $\Phi(\mathbf{r}, t) = 2kz(t)$, where $k = 2\pi f/c$ is the wavenumber, f is the frequency of the incident light beam, c is the velocity of light in vacuum and $z(t)$ is the time-dependent relative displacement along z between the emitter and the target. If the target is moving with velocity $\mathbf{v}$, the reflected signal will show an optical frequency shift $\Delta f = 2|\mathbf{v}|cos\theta/\lambda$, where θ is the angle between the velocity of the target and the direction of propagation of the light beam. Therefore, the classical Doppler effect does not provide information about the components of the velocity perpendicular to the direction of propagation of the light beam ($\theta = 90^{\circ}$).

To detect the full vector velocity, including transverse components, one can perform many Doppler measurement along the line of sight for a large set of directions[2]. Moving Doppler instruments can map the velocity field over large areas by alternating the pointing direction or by scanning the beam during the measurement. Various velocity retrieval techniques have been developed to estimate 2D and 3D vector fields from Doppler longitudinal data. Algorithms range from computationally intensive variational data assimilation techniques to simpler and faster methods based on volume velocity processing. In general, however, all these algorithms suffer poor spatial and temporal resolution and tend to lose local information about the velocity field due to the averaging involved. Moreover, these schemes requires fast mechanical realignment of the direction of propagation of the laser beam, which render its implementation more complicated.

Relativity theory shows that the Doppler effect is indeed sensitive to transverse velocities as well - *the relativistic transverse Doppler effect*[3]. Unfortunately, it yields relative frequency shifts of the order of $\sim v^2/c^2$, which renders the sought-after frequency shifts staggeringly small in all applications of interest in current laser radar systems. Moreover, it can not distinguish between different directions of movement in the transverse plane, giving all of them the same frequency shift for a given transverse velocity.

Here, we demonstrate experimentally a method[4] for directly measuring the transverse velocity component of a moving target. The method we present here can be added to the toolbox of currently used detection methods based on the Doppler effect. The velocity and position measure of a moving target can be fully measured in a more straightforward manner, with the help of a fixed single laser beam. The key idea is the use of a *structured light*

beam where each point in its transverse plane is associated with a particular value of the phase of the field. The light reflected back from a target located at a specific position will carry information about the phase at that specific location. When the particle moves across the beam, it reflects the position-dependent varying phase imprinted on the laser beam, producing a signal with a time-dependent phase at the receiver. This can also be thought of as a Doppler shift.

Along these lines, a scheme based on a rotating off-axis aperture was used to elucidate experimentally the orbital angular momentum discrete spectrum of an arbitrary light signal[5]. In this experiment, a small detector which moves across the beam captures the local electric field at the detector location, revealing information about the phase of the beam at that location. The movement of the detector translates such phase gradient into a Doppler frequency shift. In contrast to this, the so-called rotational Doppler effect[6,7] is related to a time-varying global phase change. It is generated when a light beam with orbital angular momentum traverses a rotating element which introduces a time varying global phase. The rotating element can be a Dove prism[7], or an ensemble of atoms put previously into rotation by another light beam with orbital angular momentum[8].

Currently available technology offers different possibilities to efficiently generate arbitrary spatially-shaped light beams[9]. Appropriately designed spiral phase plates[10], computer-generated holograms[11,12] and q-plates[13] play an outstanding role and can be used to produce the required phase distribution, especially for generating light beams embedded with orbital angular momentum. A suitable combination of astigmatic optical elements can also be used to generate light with different types of phase profiles[14]. Spatial light modulators have been increasingly useful in the last few years. They allow on-demand modulation of the phase of the light: one can generate and modify complex spatial phase and amplitude light patterns in a prompt and efficient manner. In our experiments we make use of a spatial light modulator.

Results

A modified Mach-Zehnder interferometer, shown in Fig. 1 (see also Methods section) is used to demonstrate the feasibility and usefulness of the method proposed. The continuous wave (CW) Helium-Neon laser light source (wavelength $\lambda = 633$ nm, power $P \sim 15$ mW), is spatially filtered and collimated to produce a beam with a Gaussian intensity profile. The first beam splitter (BS) separates the beam into a reference beam and a signal beam. The reference beam will be needed to extract the sought-after phase information from the signal beam. The signal beam acquires the required phase profile after reflection from the Spatial Light Modulator (SLM), so that the electric field amplitude of the signal beam writes

$$E(\mathbf{r},t) = [I(\mathbf{r}_\perp)]^{1/2}\exp\{ikz + \Phi(\mathbf{r}_\perp) - i2\pi ft\} \quad (1)$$

where $\mathbf{r}_\perp = (x, y)$ are transverse coordinates, $I(\mathbf{r}_\perp)$ is intensity of the beam and $\Phi(\mathbf{r}_\perp)$ is the spatially-varying phase that has been imprinted onto the beam by the SLM. This spatially-varying phase is the key tool that allows retrieval of the transverse component of the velocity of a particle. Even though arbitrary phase profiles can be generated, prior information about the specific characteristics of the movement can make the use of certain phase profiles more convenient. For instance, a rectilinear movement calls for the use of linear phase gradients, while rotational movements might be better analyzed by azimuthally-varying phase gradients.

The structured light beam illuminates a scatterer that reflects back the signal beam with a phase that depends on the specific location of the scatterer. In order to mimic different types of movements, we use a Digital Micromirror Device (DMD). A 35 μm radius disk-like particle is made of an array of 7×14 micromirrors. Each micromirror can be switched on and off with the use of a software provided by the manufacturer. By controlling which specific mirrors are in the ON or OFF states, and the timing between these states, we can simulate different types of physical trajectories and velocities of particles. This is equivalent to having a reflecting particle that is moving in the transverse plane. At each position where the particle would be located, light is reflected back to the detector, while no light is reflected elsewhere. This system is very convenient to demonstrate the feasibility of the scheme put forward here. It allows simulating different types of movements with great control of the experimentally relevant parameters such as the specific trajectory and velocity.

We retrieve the time-varying phase of the reflected signal beam by observing the time-varying intensity modulation of the interference between the reference and the signal beams. A typical record is shown in Figs. 2(a) and (b), where a signal beam of the form $E(\rho, \varphi, z) = I^{1/2}(\rho)\exp(ikz + im\varphi - i2\pi ft)$ illuminates a particle which follows a uniform circular movement. Here ρ is the radial coordinate in cylindrical coordinates, φ is the azimuthal angle and m is the winding number of the beam[15], the number of 2π jumps of the phase as one goes around φ.

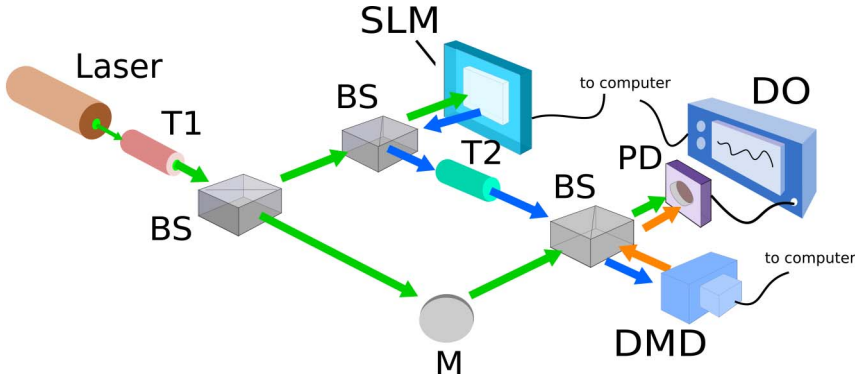

Figure 1 | The experimental set-up. A beam from a He-Ne laser ($\lambda = 632.8$ *nm*) is collimated by a telescope T1 and divided by a non-polarizing beam splitter (BS) into a reference beam (green line) and a probe beam. The probe beam impinges on a Spatial light Modulator (SLM) wherein a chosen phase profile is imprinted with a computer generated hologram. The beam (blue line) now has a structured phase profile after the SLM. The structured light is then made to shine onto a Digital Micromirror Device (DMD). The DMD is controlled to mimic a moving particle by setting which mirrors in specific positions are in the 'ON' state at a particular time. In our experiments, we turn a lump of 7×14 adjacent mirrors to the 'ON' state. This translates to a reflecting microcircle with a radius of 35 μm. We vary the speed of the movement of the particle by changing the time interval to switch to the next set of mirrors. Light reflected by the particle (orange line) is made to interfere with the reference beam at the photodetector (PD) that is attached to a digital oscilloscope (DO). The SLM, the DO and the DMD are all connected to a computer for control and for faster acquisition and analysis of data. The power ratio between the reference and the probe beam is adjusted for maximum interference fringe visibility at the PD.

Ideally, the structured optical beam is designed so that the movement of the scatterer under investigation takes place in a region where $I_0(\mathbf{r}_\perp)$ is approximately constant, so that only the spatially-varying induced phase differences produce time-varying intensity modulations at the receiver side. Finally, one obtains frequency spectra similar to Figs. 2(c) and (d) after detection, filtering and post-processing of the signal detected to remove noise and unwanted signals. The spectra give the Doppler frequency shift associated with the velocity of the scatterer.

For a given phase profile, the Doppler frequency shift due to the transverse velocity of the scatterer writes[4]

$$\Delta f = \frac{1}{2\pi}\nabla_\perp \Phi \cdot \mathbf{v} \qquad (2)$$

where $\mathbf{v}$ is the transverse velocity of the scatterer and $\nabla_\perp \Phi$ is the transverse gradient of the phase of the signal beam. Notice that Eq. (2) allows retrieval not only of the magnitude of the transverse velocity $|\mathbf{v}|$, but its direction in the transverse plane as well, since one can always produce a phase profile with a gradient along a selected direction. Fig. 3 shows results for the case of a particle moving with constant rectilinear velocity v shined by a signal beam with a uniform phase gradient profile ($\Phi(x) = \gamma x$). This uniform gradient phase profile, generated by the SLM, tilts the incident Gaussian beam into different angles[16]. The Doppler shift expected from Eq. (2) is $\Delta f = \gamma v/(2\pi)$, which shows a linear dependence on both velocity and phase gradient of the light beam. Fig. 3(a) shows the dependence of the frequency shift on the velocity of the particle for a constant phase gradient $\gamma = 17.92$ mm^{-1}, and Fig. 3(b) shows the dependence of the frequency shift for different phase gradients, for a particle that moves with velocity $v = 4.68$ mm/s.

Fig. 4 shows the case of a particle moving in a circular path with a constant angular velocity ω. In this case, the most convenient phase profile to retrieve the value of the angular velocity is the one corresponding to a Laguerre-Gauss beam with winding number m. The phase profile given by $\Phi(\varphi) = m\varphi$ has an expected Doppler shift of $\Delta f = m\omega/(2\pi)$ from Eq. (2). The Doppler frequency shift shows a linear dependence on the angular velocity and the winding number m. Fig. 4(a) shows the linear dependence of the frequency shift on the angular velocity of the target for $m = 3$, and Fig. 4(b) shows the dependence on m for a target that moves with angular velocity $\omega = 16.36\ s^{-1}$. In general, one can detect arbitrary transverse velocities by engineering phase profiles. Figs. 3 and 4 are examples of how a choice of the appropriate phase profile for a particular type of movement can give simple relationships between the velocity and the Doppler frequency shift.

Discussion

Laser Doppler instruments are widely accepted by the remote sensing community for the study of flow and particle's velocity due to its high accuracy, non-intrusiveness, directional sensitivity, and high spatial and temporal resolution. However, the classical Doppler principle only allows direct estimation of velocities along the line of sight. This research has arisen out of the need to expand the capabilities of current systems to accommodate a larger variety of applications which may benefit from information about the transverse component of the velocity not measured by classical Doppler methods.

Along these lines, the scheme demonstrated here might be added to current laser radar systems to expand their functionalities, allowing the detection of both longitudinal ($v_{||}$) and transverse components ($v_\perp$) of the velocity without the need to introduce fast changes of the pointing direction of laser beams or use several light beams. In this scenario, a properly engineered structured light beam illuminates a moving target, and the Doppler shift of the back reflected light is analyzed. Doppler signals will be generated in two different frequency bands. On one hand, the longitudinal component of the velocity will generate frequency shifts $\sim v_{||}/\lambda$. On the other hand, the transverse component will produce frequency shifts in a frequency band determined by the phase gradient of the light. For instance, a particle moving in a circular path with radius R and constant angular velocity will have a frequency shift of $\Delta f = m v_\perp/(2\pi R)$ due to the

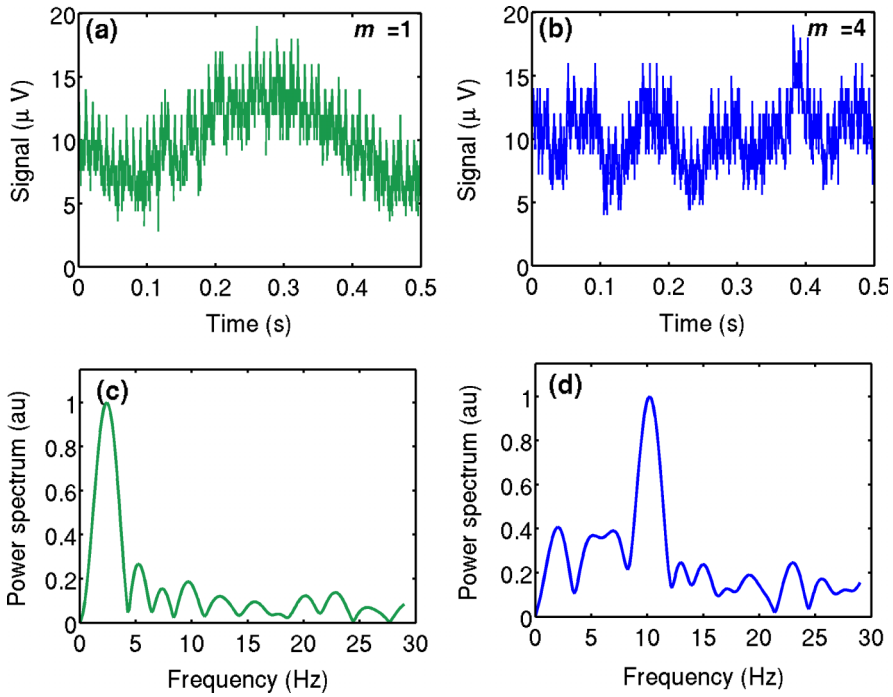

Figure 2 | Signals. Raw signals detected by the photodetector as acquired by the oscilloscope when the particle moving in a circular motion of $\omega = 16.36\ s^{-1}$, is being illuminated by a beam with a helical phase $\Phi = m\varphi$ with topological charge (a) $m = 1$ and (b) $m = 4$. Their respective power spectra (c) and (d) were obtained with an FFT algorithm. The peaks in (c) and (d) correspond to the Doppler frequency shifts of $m\omega/(2\pi) = 2.60$ *Hz* and 10.41 *Hz*, respectively. See text for further details.

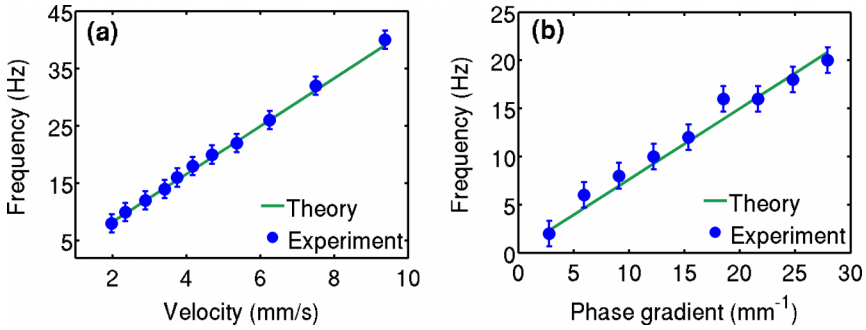

Figure 3 | Detected frequency shifts when the target moves in a rectilinear path. (a) The target is set to move at different rectilinear velocities when illuminated by a beam with a linear phase gradient of $\gamma = 17.92$ mm^{-1}. (b) The target moves under the illumination of a beam with different linear phase gradients γ at a constant linear velocity of $v = 4.68$ *mm/s*.

transverse velocity $v_\perp$. Notice that the frequency band can be tuned by changing the phase profile, which cannot be done with the classical longitudinal Doppler effect.

Notice that the magnitude of the frequency shift can be increased by changing the phase profile. In the cases shown here, the frequency can still be increased by using a higher γ for the translational movement and larger m for the rotational movement. This flexibility enables better velocity estimation as one can have a frequency that is more appropriate for different detection regimes.

The use of a spatially dependent phase gradient, which could be achieved with current technology for shaping light beams, opens the possibility to use the Doppler effect discussed here to detect not only transverse velocities, but transverse positions as well. This is because a unique phase gradient can be associated with a particular location in the transverse plane. Thereby a certain frequency shift can only come from the presence of the particle in the location with that specific phase gradient.

Recently while this paper was under review, Lavery et al.[17] demonstrated detection of the angular frequency of a spinning object by using light with orbital angular momentum. In general, the Doppler frequency shift generated by a moving surface can be written as

$$\Delta f = \frac{1}{\lambda}(\hat{\mathrm{d}}_1 - \hat{\mathrm{d}}_2)\cdot\mathbf{v} \tag{3}$$

where λ is the wavelength of the incident light with unit vector $\hat{\mathrm{d}}_1$, $\hat{\mathrm{d}}_2$ is the unit vector of the scattered light and $\mathbf{v}$ is the velocity of the moving surface[16]. For a paraxial incident beam whose vector potential[18] $\mathbf{A}$ is of the form $\boldsymbol{A} = \hat{x}\boldsymbol{u}(\boldsymbol{x},\boldsymbol{y},\boldsymbol{z})\exp(\boldsymbol{ikz})$, the Poynting vector $\mathbf{S}$ writes

$$\mathbf{S} = \frac{|\mathrm{E}|^2}{2\eta}\left(\hat{\mathrm{z}} + \frac{1}{k}\nabla_\perp\Phi\right) \tag{4}$$

where η is the vacuum impedance. Since for a paraxial beam, the longitudinal component of $\mathbf{S}$ is much larger than the transverse component, one can write

$$\hat{\mathrm{d}} = \hat{\mathrm{z}} + 1/k\nabla_\perp\Phi. \tag{5}$$

From Eqs. (3) and (5), the Doppler shift observed for $\hat{\mathrm{d}}_2 = -\hat{z}$ is

$$\Delta f = \frac{1}{\lambda}\frac{\nabla_\perp\Phi}{k}\cdot\mathbf{v} \tag{6}$$

Note that this is equivalent to Eq. (4) of Belmonte and Torres[4], which is Eq. (2) in this paper, if we substitute $k = 2\pi/\lambda$ in Eq. (6). Furthermore, we can define $\alpha \equiv 1/k\nabla_\perp\Phi$. Using $\lambda f = c$, Eq. (6) reduces to Eq. (2) in Lavery et al.[17] for a one-dimensional case. Different from the usual longitudinal Doppler effect, the frequency shift given by Eq. (4) in Belmonte and Torres[4], or Eq. (2) in Lavery et al.[17], is independent of the frequency of the illuminating light beam, and only depends on the velocity and trajectory of the object moving under structured illumination. If we illuminate the moving object with a Laguerre-Gauss beam with winding number m, the phase gradient is $\nabla_\perp\Phi = m\hat{\varphi}/\rho$. For a spinning object with velocity $\mathbf{v} = \omega\rho\hat{\varphi}$, substitution into Eq. (6) of the values of the phase gradient and velocity yields Eq. (6) in Belmonte and Torres[4] and Eq. (3) in Lavery et al.[17].

The approach proposed here can also be considered for other types of measurements, as in the case of the motility of single-cells or simple multicellular organisms. For a typical value of motility of a biological specimen of tens of micrometers per second[19], a local spatial modulation of $\sim 1\ \mu m^{-1}$ would yield a Doppler frequency shift of some tens of hertz. For instance, a typical value of the motility of sperm cells is 20 μm/s. Moreover, this scheme can also be used to measure fluid flows in live tissue, where the possibility of inducing tiny phase gradients that would not affect the in vivo system under

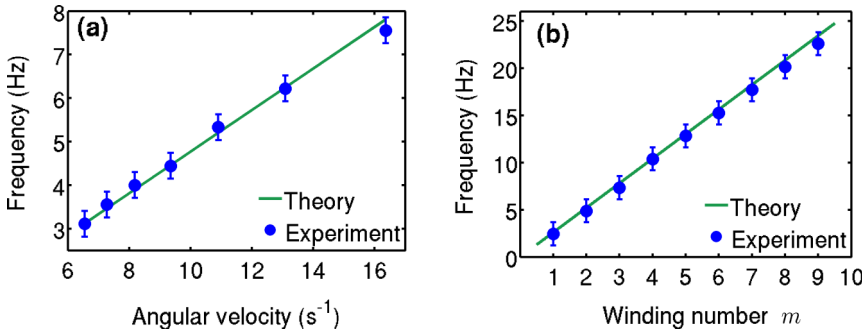

Figure 4 | Detected frequency shifts when the target moves in a circular path. (a) The target is set to move at different circular velocities when illuminated by a beam with a helical phase of $\Phi = 3\varphi$, corresponding to $m = 3$. (b) The target moves at a constant circular velocity of $\omega = 16.36\ s^{-1}$. The particle is illuminated with a phase gradient $\Phi = m\varphi$, where m is the winding number.

study can be of great interest. The diagnosis of certain important eye diseases can be assessed by observing abnormal retinal blood flow[20]. Typical blood flow velocities in the retina are in the range of some tens of mm/s. Using phase gradients of some $\sim 0.1\ \mu m^{-1}$ would result in Doppler shifts of several kilohertz.

Methods

Experimental procedure. Our experimental setup is a modified Mach-Zehnder interferometer with a 15 mW Helium-Neon laser (Melles-Griot, $\lambda = 632.8\ nm$) light source. The beam is collimated and expanded by a telescope T1 made with a lens combination of focal lengths $f = 25$ mm and $f = 100$ mm for the front and back lens, respectively. It is spatially cleaned with a 30 μm pinhole placed at the middle focus of the telescope. The beam is then divided by a beam splitter into two, a reference beam (green line in Fig. 1) and a signal beam. The signal beam impinges onto a spatial light modulator (SLM, Hamamatsu LCOS-SLM) where it acquires the desired phase profile via a 2π-modulo phase wrapped computer generated hologram (CGH) displayed on the SLM. The CGH is calculated from the interference of a beam with our desired phase and a tilted plane wave to generate a hologram with a carrier period of 84.85 μm. In our experiments, we produce beams with helical and linear phases. The helical phase is made with a phase that changes as $2\pi m$ as one goes around the azimuth, where m is an integer, the winding number of the beam. The linear phase is done by putting a small constant tilt in the beam. The carrier period makes the separation and filtering of the desired structured beam easier. This is done by appropriately placing another telescope T2 with lens combination of focal lengths $f =$ 50 mm for the front lens, $f = 30$ mm for the back lens and a 100 μm pinhole. Note that the beam size is reduced to fit into the active area of the Digital micromirror device (DMD, Texas Instruments).

The structured signal beam (blue line in Fig. 1) is then sent to the controllable DMD where a tiny circle composed of an array of micromirrors simulates a 35 μm radius particle. By manipulating the position and the time in which the mirrors are in the ON state, the micromirror ensemble can mimic a particle that is moving with different paths and velocities (see details at the Simulation of particle and its movement section). Light reflected (orange line in Fig. 1) from the DMD contains information about the velocity and position of the particle. The signal beam is then made to interfere with the reference beam at the photodetector (PD, PDAA36A-EC, Thorlabs). The PD is connected to an oscilloscope (TDS2012C, Tektronix) attached to a computer for faster data acquisition and analysis.

Simulation of particle and its movement. We control a Digital micromirror device (DMD) from a DLP Lightcrafter (Texas Instruments) to mimic a particle and its movement. We remove the RGB LED light engine to expose the DMD display. Our DMD is composed of an array of 608×684 micromirrors arranged in a diamond geometry. A single micromirror has a diagonal side length of 10.8 μm, and can be switched to an ON and OFF state. A set of 1-bit depth images are uploaded in the DMD software; a 0 corresponds to the ON state and a 1 to the OFF state. The time in which the micromirrors are in the ON or OFF state can also be controlled by the software. A micromirror in the ON state will have a tilt of $+12^\circ$ while the OFF state has -12°. Thereby, only micromirrors which are on the 'on' state will reflect light in the correct direction with a properly aligned DMD. All other micromirrors reflect light in another direction. These stray lights are blocked. We make sure that the 'ON' state reflects light parallel to the optical axis of the incident beam. We simulate a 35 μm radius particle with an array of 7×14 micromirrors. This ensemble of micromirrors are manipulated such that a constant array size are turned 'on' at specific positions in a particular interval of time while all other micromirrors are switched 'OFF'. With this, the array seems to be moving similar to a moving particle. We vary the speed of the movement by changing the time interval to switch to another set of micromirror array.

Data analysis. Understanding how the strength of our signal is distributed in the frequency domain, relative to the strengths of other unwanted ambient signals, is central to the design of any sensor system intended to estimate the signal Doppler shift. While many methods for spectrum estimation are discussed in the statistical literature, we use here only the overlapped segmented averaging of modified periodograms. In our case, a periodogram is the discrete Fourier transform (DFT) of one segment of the signal time series that has been modified by the application of a time-domain window function. It has been averaged to reduce the variance of the spectral estimates. While its practical implementation involves a number of nontrivial details -such as equal binning of frequencies, Hanning windowing, and filtering of unwanted residual amplitude modulations- our data processing and analysis is rather straightforward and computes a spectrum or spectral density starting from a digitized time series, typically measured in Volts at the input of the A/D-converter.

1. Measures, R. M. Laser Remote Sensing: Fundamentals and Applications. (Krieger Publishing Company, 1992).
2. Durst, F., Howe, B. M. & Richter, G. Laser-Doppler measurement of crosswind velocity. *Appl. Opt.* **21**, 2596–2607 (1982).
3. Sommerfeld, A. Lectures on Theoretical Physics: Optics. (Academic Press, 1954).
4. Belmonte, A. & Torres, J. P. Optical Doppler shift with structured light. *Opt. Lett.* **36**, 4437–4439 (2011).
5. Vasnetsov, M., Torres, J. P., Petrov, D. & Torner, L. Observation of the orbital angular momentum spectrum of a light beam. *Opt. Lett.* **28**, 2285–2287 (2003).
6. Courtial, J., Robertson, D. A., Dholakia, K., Allen, L. & Padgett, M. J. Rotational frequency shift of a light beam. *Phys. Rev. Lett.* **81**, 48284830 (1998).
7. Courtial, J., Dholakia, K., Robertson, D. A., Allen, L. & Padgett, M. J. Measurement of the rotational frequency shift imparted to a rotating light beam possessing orbital angular momentum. *Phys. Rev. Lett.* **80**, 3217–3219 (1998).
8. Barreiro, S., Tabosa, J. W. R., Failache, H. & Lezama, A. Spectroscopic observation of the rotational Doppler effect. *Phys. Rev. Lett.* **97**, 113601 (2006).
9. Twisted photons: applications of light with orbital angular momentum. Torres, J. P. & Torner, L. (eds.), (Wiley-VCH, Weinheim, 2011).
10. Oemrawsingh, S. *et al.* Production and characterization of spiral phase plates for optical wavelengths. *Appl. Opt.* **43**, 688–694 (2004).
11. Bazhenov, V. Y., Vasnetsov, M. V. & Soskin, M. S. Laser beams with screw dislocations in their wavefonts. *JETP Lett.* **52**, 429–431 (1990).
12. Heckenberg, N. R., McDuff, R., Smith, C. P. & White, A. G. Generation of optical phase singularities by computer generated holograms. *Opt. Lett.* **17**, 221–223 (1992).
13. Marrucci, L., Manzo, C. & Paparo, D. Optical spin-to-orbital angular momentum conversion in inhomogeneous anisotropic media. *Phys. Rev. Lett.* **96**, 163905 (2006).
14. Nienhuis, G. & Allen, L. Paraxial wave optics and harmonic oscillators. *Phys. Rev. A* **48**, 656–665 (1993).
15. Allen, L., Beijersbergen, M. W., Spreuw, R. J. C. & Woerdmann, J. P. Orbital angular momentum of light and the transformation of the Laguerre-Gauss modes. *Phys. Rev. A* **45**, 8185–8189 (1992).
16. Truax, B. T., Demarest, F. C. & Sommargren, G. E. Laser Doppler velocimeter for velocity and length measurement of moving surfaces. *Appl. Opt.* **23**, 67–73 (1984).
17. Lavery, M. P. J., Speirits, F. C., Barnett, S. & Padgett, M. J. Detection of a spinning object using light's orbital angular momentum. *Science* **341**, 537–540 (2013).
18. Allen, L., Padgett, M. J. & Babiker, M. The orbital angular momentum of light. *Progress in Optics* **39**, 291–372 (1999).
19. Chemla, Y. R. *et al.* A new study of bacterial motion: superconducting quantum interference device microscopy of magnetotactic bacteria. *Biophys. J.* **76**, 3323–3330 (1999).
20. Wang, Y., Bower, B., Izatt, J., Tan, O. & Huang, D. In vivo total retinal blood flow measurement by Fourier domain Doppler optical coherence tomography. *J. Biomed. Opt.* **12**, 041215 (2007).

Acknowledgements

We acknowledge support from the EU project PHORBITECH (FET OPEN grant number 255914), the projects funded by the Spanish government FIS2010-14831 and Severo Ochoa, and from the Fundació Privada Cellex, Barcelona.

Author contributions

C.R.G., N.H., A.B. and J.P.T. wrote the main manuscript. C.R.G. and N.H. prepared the figures. All authors reviewed the manuscript.

Additional information

Competing financial interests: The authors declare no competing financial interests.

How to cite this article: Rosales-Guzmán, C., Hermosa, N., Belmonte, A. & Torres, J.P. Experimental detection of transverse particle movement with structured light. *Sci. Rep.* **3**, 2815; DOI:10.1038/srep02815 (2013).

Nanolayer thickness detection via spatial mode projection

N. Hermosa[1,a)], C. Rosales-Guzmán[1], S. F. Pereira[2,b)], and J. P. Torres[1,3]

[1]ICFO- Institut de Ciencies Fotoniques, UPC, Mediterranean Technology Park, 08860 Castelldefels (Barcelona), Spain

[2]Optics Research Group, Delft University of Technology, Lorentzweg 1, Delft 2628 CJ, The Netherlands

[3]Department of Signal Theory and Communications, Universitat Politecnica de Catalunya, 08860, Barcelona, Spain

We demonstrate an optical scheme for measuring the thickness of thin nanolayers with the use of light beam´s spatial modes. The novelty in our scheme is the projection of the beam reflected by the sample onto a properly-tailored spatial mode. In the experiment described below, we are able to measure a step height smaller than 10 nm, i.e., one-eightieth $(1/80)$ of the wavelength with a standard error in the picometer scale. Since our scheme enhances the signal-to-noise ratio (SNR), which effectively increases the sensitivity of detection, the extension of this technique to the detection of subnanometric layer thicknesses is feasible.

The search for new optical methods to measure thickness in the range of a few nanometers or even hundreds of picometers is a topic of great interest. This is fuelled not only by the desire to reach the limit of resolution on the use of light in the nanoworld but also to develop new methods that can complement and/or substitute some well-established techniques such as X-ray spectroscopy, atomic force microscopy and ellipsometry [1,2,3]. Moreover, the continuous shrinking of all kinds of optical and electronic devices and the explosive growth of the exploration of the inner working of cells and molecular bio machines demand detection techniques that apart from being highly sensitive, must also be non-invasive, faster and easy to implement in different scenarios. These requirements can be met by photonics technologies.

Most of the time, high-resolution optical metrology is closely related to the evaluation of the phase of an electric field. In general, phases cannot be readily obtained and the desired information must be extracted indirectly by some other methods. The most widely used of these methods is interferometry. By looking at the

[a)]Author to whom correspondence should be addressed. Electronic mail: nathaniel.hermosa@icfo.es
[b)]This research was performed while S. F. Pereira was at the ICFO- Institut de Ciencies Fotoniqies, UPC, Mediterranean Technology Park, 08860 Castelldefels (Barcelona), Spain.

intensity produced at the output port of an interferometer, the relative phase can be measured and consequently, the relative thickness of a layer. Hugely small global phase differences between two independent beams up to $\sim 1\times10^{-7}$ rad can be detected [4]. The detection of small structures, such as a step[5], is more cumbersome since the reflected beam contains a spatially-varying phase instead of a global phase which should be resolved.

A major problem in interferometry is the presence of uncontrollable disturbances that can also introduce phase differences. This is especially critical when tiny phase changes are being measured. A way to circumvent this problem is by using a common path interferometer (CPI) [6,7] where an unperturbed part of the beam acts as a reference beam and travels the same path as the signal beam. CPI has been used extensively in quantitative phase measurements since Dyson's seminal paper in 1953[8]. A CPI scheme at quadrature condition (i.e, the phase difference between the reference and signal beams is centered around $\pi/2$) is very sensitive to minute changes in the phase of the signal beam [9,10]. At this condition, CPI provides a linear relationship between the observed intensity modulation and the change in the optical phase that induces the intensity change.

One successful application of CPI at quadrature condition is in spinning-disk interferometry (SDI) [9,10]. SDI is used primarily in micro immunoassay wherein specific antigens attach to engineered substrates that fulfil the quadrature condition. Unfortunately, the need to fulfil the quadrature condition may limit the use of SDI since the phase ultimately depends on the wavelength, the thickness and the index of refraction of the substrate. Moreover there are situations where the quadrature condition cannot be achieved easily, such as when the required wavelength is either not available or might damage the sample.

In this letter, we put forward a novel way to circumvent this limitation. The key point of our approach is to project the reflected signal onto appropriately tailored spatial modes (*spatial mode projection*) before its power is measured. Instead of engineering surfaces or constructing spokes or ridges such that the quadrature condition is met that condition is passed on to the mode projection detection system. We demonstrate this method in an experiment where we measured a step height that is $1/80$ of the wavelength with a standard error in the range of picometers. We also show that the power of the beam upon projection has a linear dependence with tiny height changes for any substrate with an appropriate mode. Moreover by means of spatial mode projection, the signal-to-noise (SNR) is improved compared to standard SDI. We briefly mention here that there are other optical methods which use the difference in total power detected between light that are reflected with

and without the sample to infer the thickness and refractive index of multilayers[11]. However, these methods are highly sensitive to the optical characteristics of the substrate and these do not work for low-loss highly reflecting samples.

In our scheme, the detected signal P can be written as

$$P = \eta \int r(x, y) E_i(x, y) U(x, y) dx dy \tag{1}$$

where η is the detection efficiency, $r(x, y)$ is the reflection coefficient, $E_i(x, y)$ is the incident electric field and $U(x, y)$ is the spatial mode we project onto. This projection can be efficiently made with diverse optical devices such as computer-generated holograms in spatial light modulators or liquid crystal switchable plates. The selection of mode to project onto the reflected light depends on the geometry of the sample. For simplicity, but without any loss of generality, we use a step sample in all our experiments. We define a step as a sharp discontinuity of height h of the reflecting surface.

When a Gaussian mode illuminates a step, the most appropriate modes for projection are also Gaussian modes of the form

$$\begin{aligned} U(x, y) &\sim \exp\left(-\frac{x^2 + y^2}{w_0^2} \right) \qquad x \le 0 \\ U(x, y) &\sim \exp\left(-\frac{x^2 + y^2}{w_0^2} \right) \exp(i\Delta\varphi) \quad x > 0 \end{aligned} \tag{2}$$

where w_0 is the waist of the beam and $\Delta\varphi$ is the relative phase difference between the two regions of the modes with which we project onto. When a Gaussian beam reflects from this sample and is projected on the mode given by Eq. (2), the normalized detected intensity is given by

$$P_{-\Delta\varphi} = \frac{1}{2}\left(1 + \cos(\delta + \Delta\varphi)\right) \tag{3}$$

where δ is related to the height of the cliff as $\delta = 4\pi h/\lambda$. Note that Eq. (3) is derived when the discontinuity in the phase of the mode coincides with the position of the cliff. We use Eq. (3) to measure samples with different step heights.

The experimental setup is shown in Fig. 1. A collimated HeNe laser (λ = 632.8 nm, w_0 = 1.1mm) is incident on a sample with a step height of h. Our samples are etched SiO_2 on top of a Si wafer. We image the reflected light with a telescope onto the Spatial Light Modulator (SLM, Hamamatsu). The SLM is controlled to have a phase profile as in Eq (2). This is done by using appropriate 8-bit gray level values. Each gray level corresponds to a particular value of phase that the beam will acquire. Half of the beam acquires a phase of $\Delta\varphi$ with respect to its other half. The beam after the SLM is then sent to the single mode fiber (SMF). The SMF is connected to a Si photodector that is attached to a lock-in amplifier system. The laser beam is chopped before the sample and its chopping frequency is used as the reference frequency of the lock-in amplifier. The chopping frequency used is 3 kHz and the integration time of the lock-in amplifier is 300 ms. The data are logged by a digital oscilloscope (DO, Agilent) to the computer. In our measurements, we have also obtained the normalized intensity $P_{-\Delta\varphi}$, the power reflected for a phase $-\Delta\varphi$. This is done by switching the gray level values of the two regions of the SLM.

Figure 2 shows our experimental results for different step heights. Note the good correspondence of the experimental curve with the theoretical calculations. The values used for the theoretical curves are 0 nm, 8 nm and 31 nm, respectively. These are measured by a commercial profilometer (Alpha-Step IQ Surface profilometer). To quantify the height of the step from our measurements, we take the difference between $P_{\Delta\varphi}$ and $P_{-\Delta\varphi}$. The difference of the normalized powers is given by

$$P_{-\Delta\varphi} - P_{\Delta\varphi} = \sin\delta \sin\Delta\varphi . \qquad (4)$$

Note that the step height is readily accessible with $\sin\delta$ as $P_{-\Delta\varphi} - P_{\Delta\varphi}$ is plotted as a function of $\sin\Delta\varphi$. The uncertainty in the measured height comes from the standard error of the slope of the plotted line.

Figure 3 is an example of the analysis done to the experimental data. The experimental results fit nicely to the data. No fitting parameters are used. The maximum amplitude happens at quadrature $\Delta\varphi = \pi/2$ as seen in Fig. 3(a). The measured thickness layers are summarized in Table I. The uncertainty comes from the fact that the sample is not smooth as observed in the profilometer scans (*not shown*). Moreover, we ascribe the 1.9 nm offset in our data to the existence of a nonlinear relationship between the gray level value and the phase

introduced by the SLM near π which we found during initial calibration of the SLM (see for example the difference in the line fit with the theoretical line in Fig 3(b) near π).

As in the SDI, the maximum sensitivity in our scheme happens at the quadrature condition. The main difference, however, is the detection scheme. Consider for example a step geometry that fulfils the quadrature condition with a thin layer sample placed on top of the step. The system is illuminated by a Gaussian beam with beam waist w_0 and power P_0. The signal of interest is the normalized differential signal $P_1 - P_2$ where P_1 and P_2 are the power of the detected signal from the step with and without the thin layer. In the SDI, there is an optimum area of detection that gives the maximum value of $P_1 - P_2$. Increasing the area of detection decreases $P_1 - P_2$. In the mode projection scheme on the other hand, the total power of the projected signal is measured and hence, the power does not depend on the detection area. More importantly, given the proper choice of mode the signal-to-noise ratio will be higher. In the step geometry considering shot-noise condition, the SNR ratio is enhanced by ~ 2 dB compared to SDI when using spatial mode projection with $\Delta\varphi = 0$.

The importance of the quadrature condition is the large linear change in the differential signal produced by a tiny layer if the substrate is at quadrature. When the system is not at quadrature, the differential signal is diminished dramatically. This is not an issue in the scheme we present here as spatial modes can be easily engineered such that the linear dependence of the normalized differential signal $P_1 - P_2$ is preserved for any optical height h/λ. We show this for a thin layer on top of a flat substrate (inset Fig 4). In this case, the SDI will not work since the thin layer is on top of a substrate that does not meet the quadrature condition. In our scheme we can re-introduce the quadrature condition on the mode. Fig. 4 shows the differential signal when the reflected signals are projected onto Gaussian modes with different phase steps. Notice that at $\Delta\varphi = \pi/2$, the differential signal is linear with the height of the layer at the same time giving the maximum differential signal. On the contrary, $\Delta\varphi = \pi/4$ and $\Delta\varphi = 0$ do not give optimal differential signals. This is what we observe in our experiment (Fig. 3(a)). We note however that similar to SDI, the lateral resolution of our technique is diffraction limited.

The measurement of subnanometric steps requires the detection of small power differences $P_1 - P_2$. In our scheme, a normalized height $h/\lambda \sim 10^{-4}$ and an initial laser power of 1 mW would give a differential

signal of $\delta/2 \sim 600\,\mathrm{nW}$. This differential signal can be detected in principle. One can use the intensity measurement method by Freudiger et al. [12], where a high frequency detection scheme is used to get rid of lower-frequency laser noise, thus allowing the detection of a fractional power losses of up to $\sim 10^{-7}$. The signal–to–noise ratio is $S/N = \delta/2\sqrt{2\pi E\lambda/2\hbar c} \sim 14\,\mathrm{dB}$ in our scheme using the parameters above.

In conclusion, we have demonstrated that extremely small step heights can be measured without the need to impose stringent conditions on the substrate by using spatial mode projection in a common path interferometer. We have measured a layer thickness as low as 9.7 nm with a standard error of 170 pm in our experiment. Moreover, we have shown that our scheme enhances the sensitivity of detection and hence, can also be used for subnanometric step height measurements.

This work was supported by the Government of Spain (project FIS2010-14831 and the program Excelencia Severo Ochoa), the European project PHORBITECH (FET-Open grant number: 255914), and the Fundacio Privada Cellex Barcelona. S.F.P. is grateful to ICFO for hosting her 6-month stay. Johan Osmond did the profilometry measurements.

FIGURES and TABLE

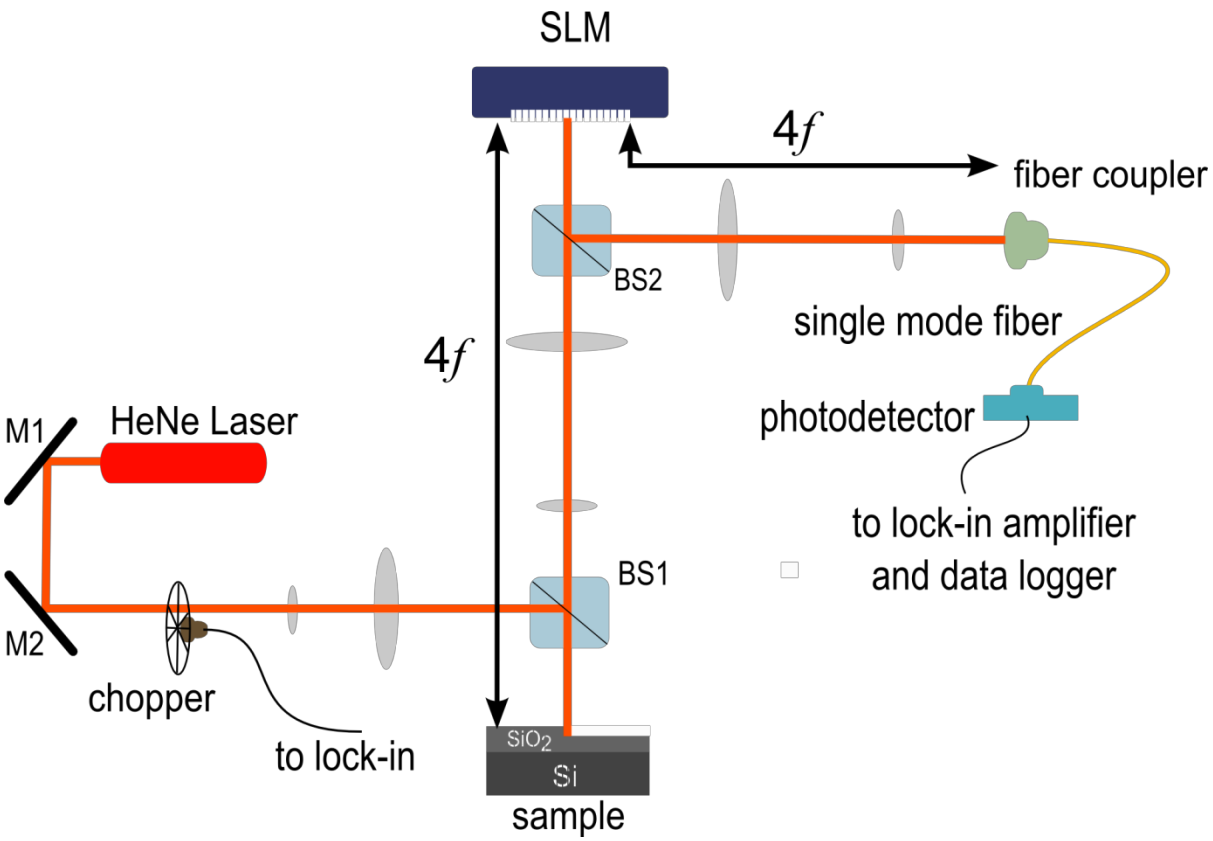

FIG 1. (Color online). The experimental setup. A HeNe laser beam impinges perpendicularly to the sample (the diagram of the sample is exaggerated). The reflection from the sample is then projected onto an SLM where a desired phase is encoded. The resulting beam is sent to a single mode fiber. A lockin amplifier with a chopper is used to lessen technical noise. *See text for details*.

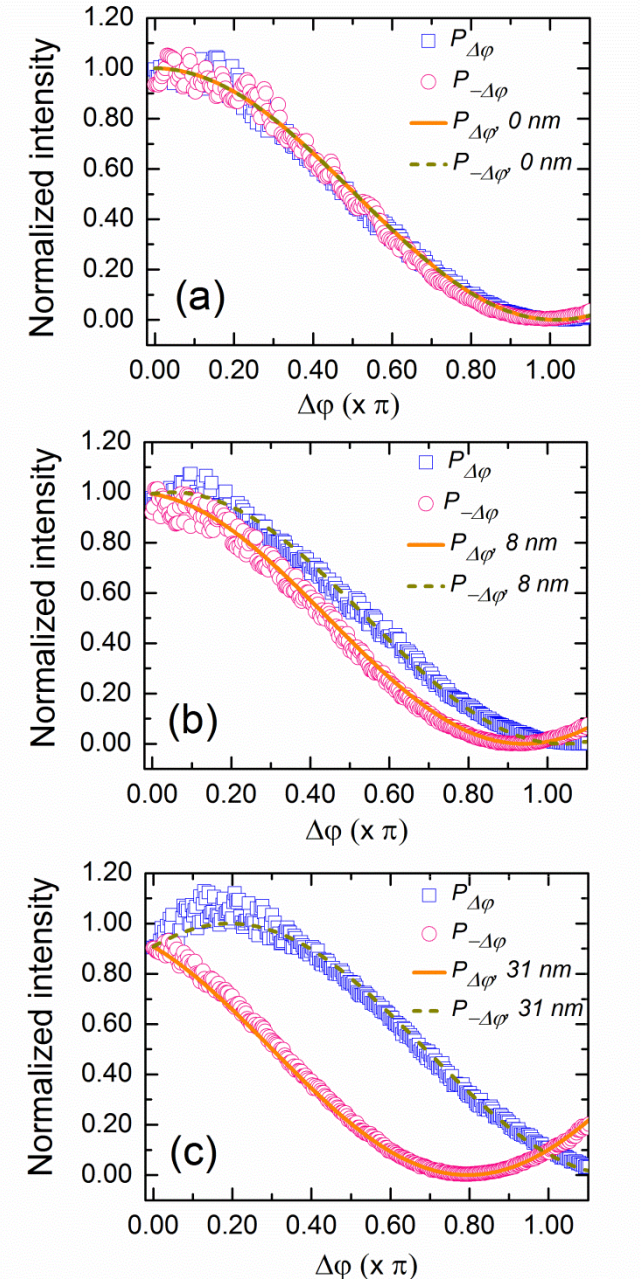

FIG 2. (Color online) Normalized intensities for P when projected onto a mode of phases $\Delta\varphi$ and $-\Delta\varphi$ for different heights: (a) 1.9 nm for sample 1, (b) 9.7 nm for sample 2 and (c) 29.0 for sample 3. All measurements have standard error of 0.2 nm. The measurements based on the experimental data is discussed in the text. Theoretical curves where calculated based on the measurement done with a commercial profilometer.

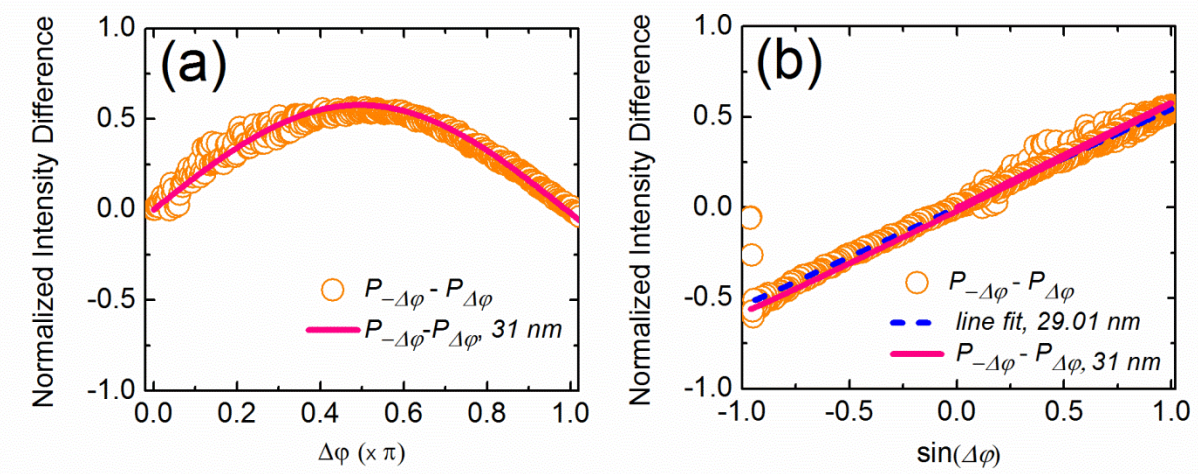

FIG. 3. (Color online) Typical data for analysis. (a) Normalized power difference $P_{\Delta\varphi} - P_{-\Delta\varphi}$ as a function of $\Delta\varphi$. (b) The difference as a function of $\sin(\Delta\varphi)$ is linear as described by Eq. (4). Line fit is from the calculated height (dashed line) and from theoretical calculations (solid line). For all plots, the theoretical curve is calculated from a cliff height of 31 nm which is independently measured with a profilometer.

Table I . Experimental thickness layer (in nanometers)

	Profilometry[a]	*CPI with mode projection*[b]	*Std Err*
Sample 1	*0*	*1.89*	*0.23*
Sample 2	*8*	*9.72*	*0.17*
Sample 3	*31*	*29.01*	*0.21*

[a]Alpha-Step IQ Surface profilometer. The standard error in the height obtained with the profilometer is in order of nanometers (~1-2 nms) owing to the uneven surface of the sample.

[b]The offset of ~ 1.89 nm is due to the nonlinear relationship between the gray level value of an image and the phase that the SLM renders.

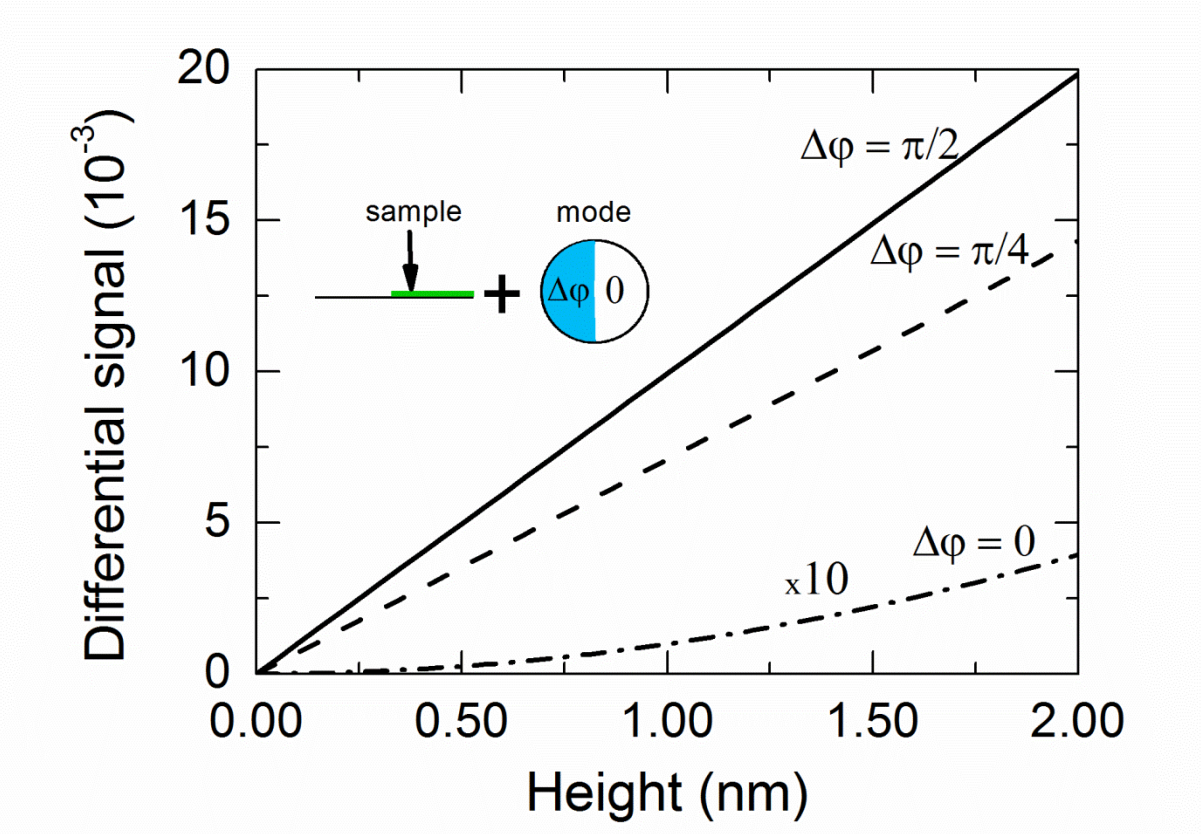

FIG 4. (Color online) Normalized differential signal $\beta_1 - \beta_2$ as a function of the sample height when the reflected signal is projected onto a Gaussian mode with phase step $\Delta\varphi$. The solid, dash and dash-dotted (× 10) lines correspond to $\Delta\varphi = \pi/2, \pi/4, 0$, respectively.

REFERENCES:

[1] Z. H. Lu, J. P. McCaffrey, B. Brar, G. D. Wilk, R. M. Wallace, L. C. Feldman and S. P. Tay, Appl. Phys. Lett. **71**, 2764 (1997).

[2] H.-U. Danzebrink and L. Koenders and G. Wilkening and A. Yacoot and H. Kunzmannl, CIRP Annals-Manufacturing Technology **55**, 841-878 (2006).

[3] M. Losurdo, M.Bergmair, G. Bruno, D. Cattelan, C. Cobet, A. de Martino, K. Fleischer, Z. Dohcevic-Mitrovic, N. Esser, M. Galliet, R. Gajic, D. Hemzal, K. Hingerl, J. Humlicek, R. Ossikovski, Z. V. Popovic, and O. Saxl, J. Nanopart. Res. **11**, 1521-1554 (2009).

[4] N. Matsuda, R. Shimizu, Y. Mitsumori, H. Kosaka and K. Edamatsu, Nat. Photon. **3**, 9 (2009); N. Matsuda, Y. Mitsumori, H. Kosaka, K. Edamatsu, and R. Shimizu, Appl. Phys. Lett. **91**,171119 (2007).

[5] S. Furhapter , A. Jesacher, S. Bernet and M. Ritsch-Marte, Opt. Express **13**, 689 (2005).

[6] J. Dyson, J. Opt. Soc. Am. **47**, 386-562 (1957).

[7] J. Glückstad, and P.C. Mogensen, Appl. Opt. **40**, 268-282 (2001).

[8] J. Dyson, Nature **171**, 742-744 (1953).

[9] M. Zhao, W. Cho, F.E. Regnier, and D.D. Nolte, Appl. Opt. **26**, 6196-6209 (2007).

[10] M. M. Varma, H.D. Inerowicz, F.E. Regnier, D.D. Nolte, Opt. Lett. **29**, 950-952 (2004); M. M. Varma, H.D. Inerowicz, F.E. Regnier, D.D. Nolte, Biosens. Bioelectron. **19**, 1371-1376 (2004).

[11] B. P. Blake, E. W. Hill, A. H. Castro Neto, K. S. Novoselov, D. Jiang, R. Yang, T. J. Booth, and A. K. Geim, Appl. Phys. Lett. 91, 063124 (2007).

[12] C.W. Freudiger, W. Min, B.G. Saar, S. Lu, G.R. Holtom, C. He, J.C. Tsai, J.X. Kang, and X.S. Xie, Science **322**, 1857 (2008); B.G. Saar, C.W. Freudiger, J. Reichman, C.M. Stanley, G.R. Holtom, and X.S. Xie, Science **330**, 1368 (2010).